Supplementary information

Sustainable Solar-Driven Synthesis of High-Purity Carbon Quantum Dots from Corn Stover for Efficient H_2O_2 Production from Water

Xuejing Kang[a], Qian Yang[b], Sean Xiang Tang[a], Zhe Chen[a], Samir Budhathoki[a], Ramhari Paneru[a], Soyoung Kim[g], Yan Bai[c], Qian Li[c], Zhongbing Chen[d], Alexander Goroncy[e], Richard N. Zare[f*], Maohong Fan[g,h*]

[a] Department of Energy & Petroleum Engineering, University of Wyoming, Laramie, WY 82071, USA
[b] Center for Advanced Scientific instrumentation, University of Wyoming, Laramie, WY 82071, USA
[c] College of Chemistry and Chemical Engineering, Henan University, Kaifeng, Henan 475004, P.R. China
[d] Department of Applied Ecology, Faculty of Environmental Sciences, Czech University of Life Sciences Prague, Kamýcká 129, 16500 Praha-Suchdol, Czech Republic
[e] Department of Chemistry, University of Wyoming, Laramie, WY 82071, USA
[f] Department of Chemistry, Stanford University, Stanford, CA 94305, USA.
[g] College of Engineering and Physical Sciences, and School of Energy Resources, University of Wyoming, Laramie, WY 82071, USA
[h] College of Engineering, Georgia Institute of Technology, Atlanta, GA 30332, USA
*Corresponding authors: Richard N. Zare and Maohong Fan
Email: zare@stanford.edu; mfan@uwyo.edu.

Contents

Text S1. Effect of light intensity

The corn stover-derived CQDs were prepared within 24 hours and were vigorously stirred using various light intensities of 555 mW/cm², 834 mW/cm², and 1050 mW/cm², respectively (Table S1, *Samples 1-3*). Figure S2 (a-c) displays the 3D-EEM fluorescence spectra of the synthesized samples, and it can be observed that all the prepared solutions displayed weak fluorescence properties. However, the solution prepared with a light intensity of 834 mw/cm² showed a stronger photoluminescence effect than the others. The pH values of the prepared samples (Table S1) showed no noticeable change under different light intensities. Figure S2(d) shows that the UV absorption peaks appear at 232 nm and ~278 nm. The absorption peak at 232 nm was due to the π-π* transition of C=C, while the strong absorption of CQDs in the region of 250-300 nm is preferably considered 'n to π*' transitions of C=O. Figure S2 (f) shows the temperature trends at different light intensities. The temperatures of all samples became stable after 4 hours of light irradiation.

Text S2. Effect of reaction time

The CQD samples were prepared using vigorous stirring and a light intensity of 834 mW/cm², with reaction times varying from 24 h to 120 h (Table S1, Samples 2-*7*). Figure S3 (a-e) displays the 3D-EEM fluorescence spectra of the samples. With an increase in reaction time, the photoluminescence effects of the samples were enhanced by an increase in emission intensity, centered at Ex/Em = 350-370 nm / 440-460 nm. Higher intensity is generally caused by the higher concentration of the fluorescent CQDs, resulting from more ordered and uniform aromatic structures. The aqueous sample with the strongest photoluminescence effect was discovered when the reaction time was 96 hours. Although the reaction time exceeded 96 hours, the compounds that were dissolved in the solution likely became an obstacle to the light, and further reactions might be impeded.

The pH values (Table S1) of the prepared samples exhibited a clear decreasing trend. At the same time, the reaction times increased, indicating the yield of the organic acids (-COOH) gradually increased as the reaction proceeded. The temperature of the samples (Figure S3(f)) was approximately 50°C, which is consistent with the results shown in Figure S2(e).

Figure S3(g) shows that the UV absorption peaks appeared at 232 nm and ~270-290 nm. The absorption peak at 232 nm was due to the π-π* transition of C=C, while the strong absorption of CQDs in the region of 250-300 nm is preferably considered to be 'n to π*' transitions of C=O.

Figure S3(h) compares the FTIR spectra of CQD samples prepared at 24 h, 48 h, 72 h, 96 h, 120 h. The broad absorption band at about 3500-3000 cm^{-1} is attributed to the stretching vibration of

O-H and N-H bonds[1,2]. The peak at 2930 cm^{-1} originated from C-H while C=C, C-O and C-O-C were observed at 1580 cm^{-1}, 1243 cm^{-1} and1029 cm^{-1}, respectively [3–5]. Particularly, C=O could be observed at 1690-1740 cm^{-1}. The C=O bond formed when the reaction time exceeded 96 hours, whereas it was not obvious when the samples were prepared with less than 96 hours.

Text S3. Effect of O_2 flow

In this part, the CQDs were prepared under the conditions of strong stirring, a light intensity of 834 MW/cm^2, and a reaction time of 96 hours, while varying the O_2 flow rate from 0 to 42 mL/min (Table S1, *Samples 8-11*). Figure S4 (a-d) displays the 3D-EEM fluorescence spectra of the CQDs. As the O_2 flow rate increased, the fluorescent properties of the samples also enhanced, in line with the rise in O_2 flow rate. However, the sample with a flow rate of 40 mL/min exhibited poorer performance than the others, which may be due to the excessive amount of O2 interfering with the Fenton reactions or enhancing the condensation reactions, leading to an increase in the carbon quantum dots. Compared with the sample synthesized, the pH of the samples prepared within an O_2-rich atmosphere showed a drastic drop, which was approximately 4 (Table S1), demonstrating that O2 accelerated the degradation of organics from corn stover and the formation of organic acid (-COOH).

Figure S4 (e) and Figure S4 (f) compared the UV-vis absorption and FTIR spectra of the prepared CQD samples with different O_2 flow rates, respectively. The peaks in UV absorption and FTIR were consistent with the results shown in Figures S3 (g) and S3 (h).

Text S4. Effect of light wavenumber ranges

To prepare CQDs at different light wavelength ranges (Table S1, *Samples 12-14*), the simulated solar light was filtered by the parallel optical filters with the transmittance ranges of 250 - 430 nm, 430 - 700 nm and 650 - 1000nm (Parallel Optical Window, Newport, USA, model: FSW18AR.10; 20BW40-30; 20QW40-30AR.16), under the conditions of strong stirring and reaction time of 96h. Figure S5 (a-d) displays the 3D-EEM fluorescence spectra of the CQDs. The emission intensities of the CQDs prepared with UV and infrared lights are higher than those prepared with only visible light. This might be because UV light possesses higher photon energies, and infrared light provides more thermal energy than visible light.

Text S5. Effect of separated components of corn stover

Corn stover mainly comprises cellulose, hemicellulose, and lignin [6]. The experiments (Table S1, *Samples 15-17*) were performed at the same experimental setup and conditions to compare the difference between the corn stover and a single component for CQDs synthesis. The poor

fluorescent properties of the samples may be due to the lack of iron ions, which results in a reduced oxidative power of the solution. Figure S6 also indicated that cellulose was hardly degraded, while lignin and hemicellulose were oxidatively degraded.

Text S6. Additional control experiments

To further evaluate the individual roles of illumination, temperature, and oxygen availability, two additional control reactions were performed. In *Sample 18* (dark + O_2), the reactor was supplied continuously with O_2 (28 mL min^{-1}) while completely shielded from light; the reaction remained near ambient temperature because no external heating or illumination was applied. In *Sample 19* (light + N_2), the reactor was illuminated under simulated solar light but supplied with N_2 instead of O_2. The corresponding 3D excitation–emission fluorescence spectra for these controls are presented in Figure S7, which complements the fluorescence results reported for *Sample 6* (light + no added gas, Figure S3d), *Sample 10* (light + O_2, Figure S4c), and *Sample 8* (dark + external heating, Figure 1g).

Text S7. ESR measurement

Electron spin resonance (ESR) measurements were performed on a Bruker EMX EPR spectrometer (X-band) using 5,5-dimethyl-1-pyrroline N-oxide (DMPO) as a spin-trapping agent to detect transient reactive oxygen species. Spectra were recorded at a microwave frequency of ~9.87 GHz, with a center magnetic field of 3514 G, sweep width of 100 G, modulation frequency of 100 kHz, modulation amplitude of 7 G, and microwave attenuation of 38 dB. The time constant and conversion time were both set to 20.48 ms.

Unless otherwise noted, ESR samples were prepared by mixing 50 μL of reaction solution with 50 μL of 1.6 M DMPO immediately before to analysis. For selected control experiments, 3 μL of a 5 mM Fe^{2+} solution was added just before measurement as a diagnostic trigger to promote Fenton-type conversion of accumulated peroxide into hydroxyl radicals. Fe^{2+} was introduced only during ESR measurements and was not added during photocatalytic operation or material synthesis, where trace metal species originate naturally from the biomass matrix.

Text S8. Fenton and Fenton-like reactions

Fenton and Fenton-like oxidation are considered advanced oxidation processes (AOPs) that involve radical-based reactions, where redox interactions occur between multivalent metals and reactive species. These processes are well-regarded for their high efficiency in degrading organic pollutants. In these systems, multivalent metals act as essential catalysts, such as Fe, Cu, Co, Mn, Ce, Ag, Cr, Ru, W, Mo, V, and Ti [7]. They facilitate the activation of hydrogen peroxide (H_2O_2),

generating reactive oxygen species (ROS) that can break down complex organic compounds. At the same time, the dual roles of H_2O_2 as both a reductant and oxidant enable it to interact with low-valent metals (M^{n+}) possessing reducing properties and high-valent metals ($M^{(n+z)+}$) exhibiting oxidizing properties. This dynamic redox mechanism leads to the efficient production of ROS, such as hydroxyl radicals (•OH), which are crucial for the oxidative degradation of organics in various environmental and industrial applications [7]. For example, when Mn or Cu is the catalyst, the mechanism equations of Fenton-like reactions are as follows[8]:

$$Mn^{2+} + H_2O_2 \rightarrow Mn^{3+} + OH\bullet + HO^- \quad \text{(SR1)}$$
$$Mn^{3+} + H_2O_2 \rightarrow Mn^{2+} + HO_2\bullet + H^+ \quad \text{(SR2)}$$
$$Cu^{+} + H_2O_2 \rightarrow Cu^{2+} + OH\bullet + HO^- \quad \text{(SR3)}$$
$$Cu^{2+} + H_2O_2 \rightarrow Cu^{+} + HO_2\bullet + H^+ \quad \text{(SR4)}$$

The elemental analysis results for three CQD samples (*S6, S8, and S10*) are presented in Table S3, focusing on the concentrations of transition metals that may facilitate Fenton or Fenton-like reactions. Notably, iron (Fe), copper (Cu), and manganese (Mn) — the key catalysts for classic and non-classic Fenton processes — were detected in all samples. Fe concentrations ranged from 0.14 to 0.81 ppm, Cu from 0.03 to 0.32 ppm, and Mn from 0.01 to 0.25 ppm, indicating their consistent presence in the CQD matrix. These metals are well-known for their ability to activate hydrogen peroxide, generating ROS such as hydroxyl radicals, which supports the potential for oxidative degradation pathways in this system. Additionally, trace levels of cobalt (Co), chromium (Cr), and nickel (Ni), which may also contribute to Fenton-like mechanisms under specific conditions, were observed. The detection of these redox-active elements strongly supports the hypothesis that both Fenton and Fenton-like reactions are feasible within the CQD environment, enhancing its potential for catalytic or environmental applications.

Text S9. Thermogravimetric analysis

The thermogravimetric analysis (TGA) of both the raw biomass (corn stover) and the derived CQDs (*sample 10*) was evaluated using a simultaneous thermal analyzer (DSC/TGA SDT Q600). The corn stover powder was analyzed under a nitrogen atmosphere from room temperature to 750 °C, followed by heating in air from 750 to 900 °C, at a constant heating rate of 10 °C/min. The sample was held isothermally for 60 minutes at both 750 °C and 900 °C to ensure complete decomposition and combustion.

For the CQD product, the analysis was conducted under nitrogen from room temperature to 50 °C at a heating rate of 10 °C/min, followed by an isothermal hold at 50 °C for 180 minutes to assess low-temperature volatility. The sample was then heated in air to 900 °C, with 60-minute holds at both 750 °C and 900 °C to fully oxidize any remaining material.

The TGA results of the corn stover powder and the derived CQDs) are presented in Figure S10a and S9b, respectively. For the corn stover powder (Figure S10a), an initial weight loss of approximately 5.42% occurred at 100 °C, corresponding to the evaporation of moisture and light volatile components. A major weight loss of 71.62% was observed around 374 °C, which is attributed to the thermal decomposition of hemicellulose, cellulose, and lignin, the primary constituents of lignocellulosic biomass. After pyrolysis in a nitrogen atmosphere up to 750 °C, a residual ash content of 2.41% remained. Subsequent combustion in air up to 900 °C led to a slight increase in residue to 2.97%, indicating minor oxidation of the remaining carbonaceous material.

In contrast, the CQD sample (Figure S10b) exhibited rapid and nearly complete weight loss below 150 °C, suggesting a high proportion of volatile or low-molecular-weight organic species. A prolonged isothermal hold at 50 °C for 180 minutes with only 0.51% dry weight remaining. Following pyrolysis and high-temperature combustion, the final ash content was extremely low (0.04%), reflecting the high purity and minimal inorganic residue of the synthesized CQDs.

Text S10. Centrifuge and dialysis procedure for CQDs

The CQD solution was first passed through a 0.22 μm syringe filter to remove large particulates. It was then centrifuged at 10,000 rpm for 10 minutes using an Eppendorf Centrifuge 5418 (USA) to remove aggregates and insoluble residues. The CQD solution was then transferred into a dialysis bag with a molecular weight cut-off (MWCO) of 1000 Da. The bag was immersed in deionized (DI) water and maintained at room temperature under gentle stirring. To ensure effective removal of small molecular weight impurities, the DI water was replaced every 24 hours**.** The dialysis process was continued for a total of 3 days. After completion, the dialyzed CQD solution was collected for further characterization.

Text S11. Evaluation of CQDs purity

CQD solutions before (Figure S11, black) and after dialysis (Figure S11, blue) were separately analyzed by liquid chromatography–mass spectrometry (LC-MS) to evaluate the removal of small molecular weight impurities. LC-MS analysis was performed using an Agilent 1260 Infinity HPLC system coupled with a 6120 Quadrupole MS, equipped with a Hi-Plex H column at 50 °C, with water as the mobile phase at a flow rate of 0.6 mL/min. The chromatographic run was carried out over 60 minutes, and data were collected in negative ion mode. The results demonstrate that dialysis successfully removed small molecular fragments formed during CQD synthesis, enhancing sample purity, as indicated by the marked reduction in peak intensities following treatment.

Table S5 summarizes the ICP-MS and ion chromatography (IC) results for the CQD solution (S-10) after purification by centrifugation and dialysis filtration, providing clear evidence of the

sample's high purity. Most metal ions, including Ag, Ce, Co, Ni, Pb, Ru, Ti, V, and W, were completely removed (0.00 ppm), while only trace amounts of Al (0.04 ppm), Cr (0.01 ppm), Cu (0.06 ppm), Fe (0.07 ppm), Mn (0.02 ppm), and Mo (0.03 ppm) remained. These residual concentrations collectively account for only 0.23 ppm of total metal ions, indicating highly effective purification. Notably, the presence of Fe, Cu, and Mn—despite being at trace levels—still supports the potential for Fenton and Fenton-like reactions within the CQD system. Regarding anionic species, the IC analysis shows that all detected ions (F^-, NO_3^-, Br^-, PO_4^{3-}) were not detected (0.00 ppm), except for Cl^- (1.18 ppm) and SO_4^{2-} (0.53 ppm), resulting in a total ionic content of only 1.71 ppm. This very low concentration of residual cations and anions strongly demonstrates the high purity of the CQD solution after the purification process, making it well-suited for applications requiring minimal interference from impurities, such as photocatalysis or bioimaging.

Figures and tables

Figure S1. Experiment strategy, setups, and H_2O_2 test results of the system

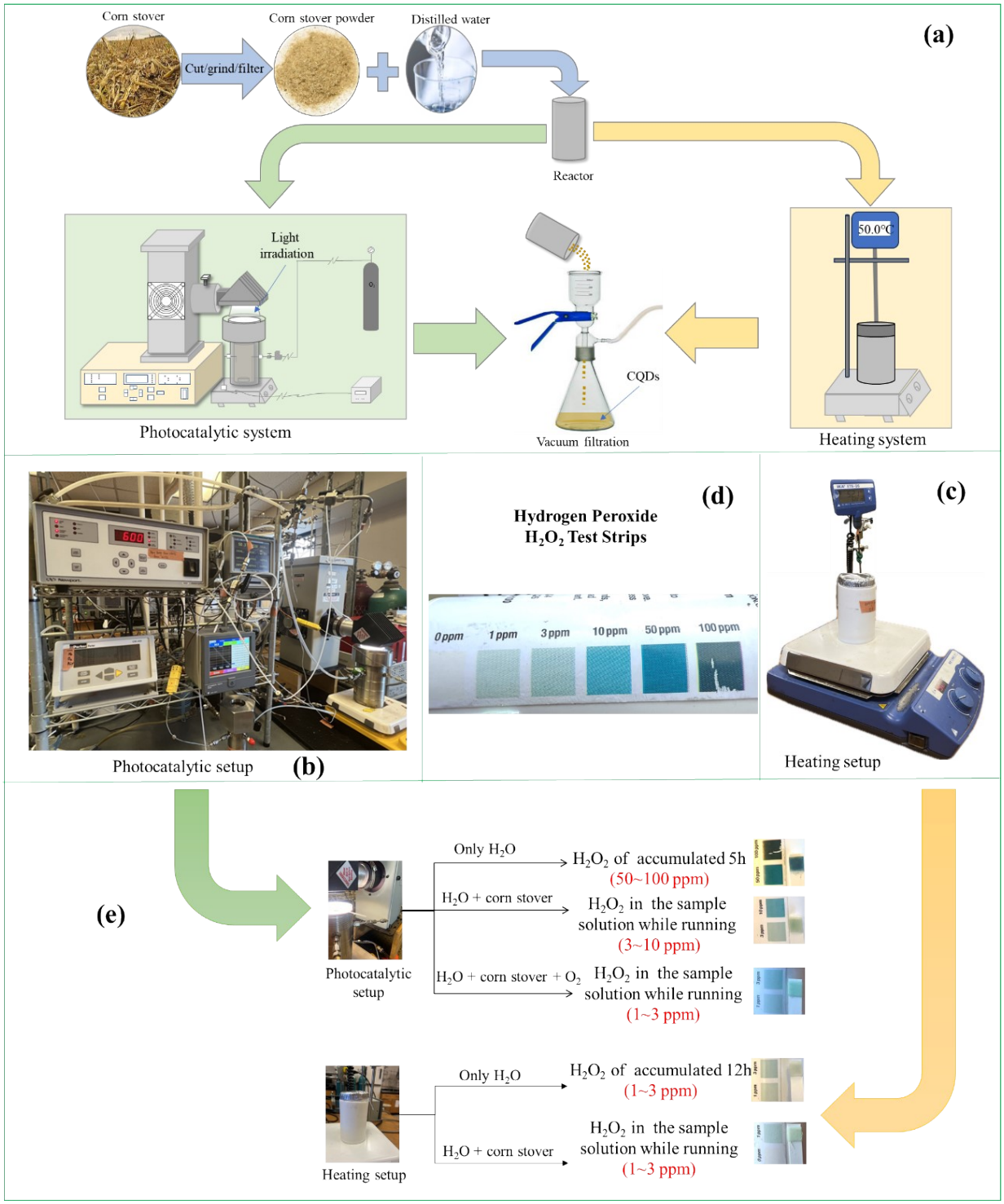

Figure S1. (a) Schematic illustration of the formation of fluorescent CQDs from corn stover via light irradiation; (b) Photocatalytic setup for CQDs synthesis; (c) Heating setup for CQDs synthesis; (d) H_2O_2 test strips used in this work; (e) the H_2O_2 test result under different conditions of the system.

Figure S2. Effect of light intensity

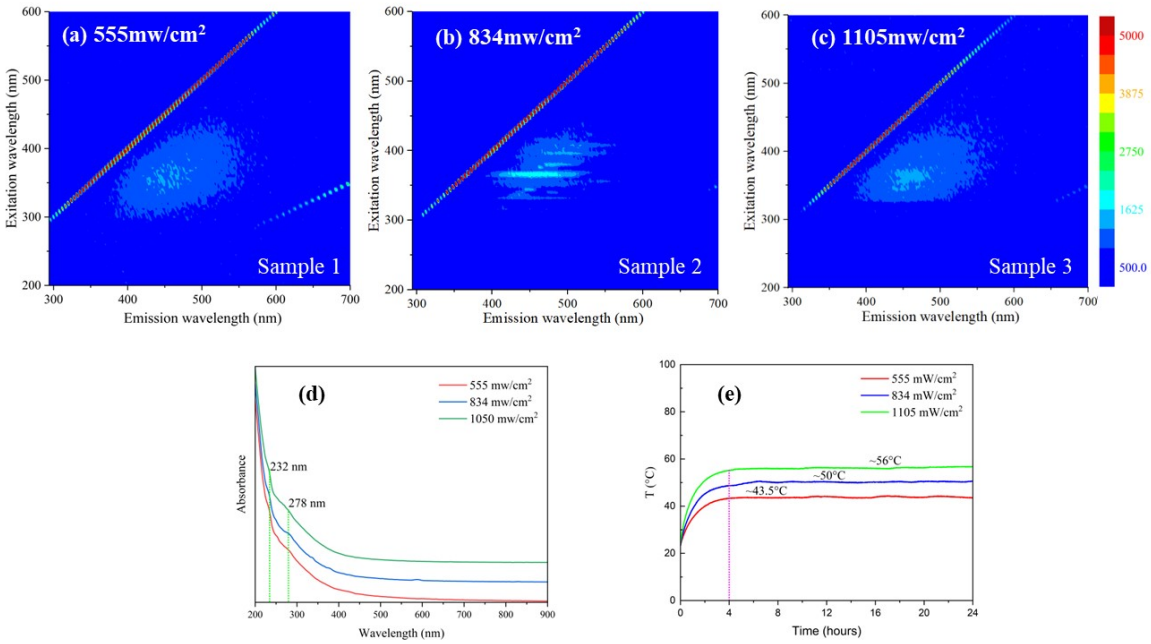

Figure S2. 3D emission-excitation-intensity spectra of CQDs synthesized at the light intensity of (a) 555 mW/cm^2 (450 W); (b) 834 mW/cm^2 (600 W); (c) 1050 mW/cm^2 (750 W); (d) Comparison of UV-vis absorption spectra of CQDs based on various light intensity; (e) Comparison of temperature of CQDs synthesized with different light intensity. (Other reaction conditions: 24 h of reaction time, strong stirring, with an atmosphere environment).

Figure S3. Effect of reaction time

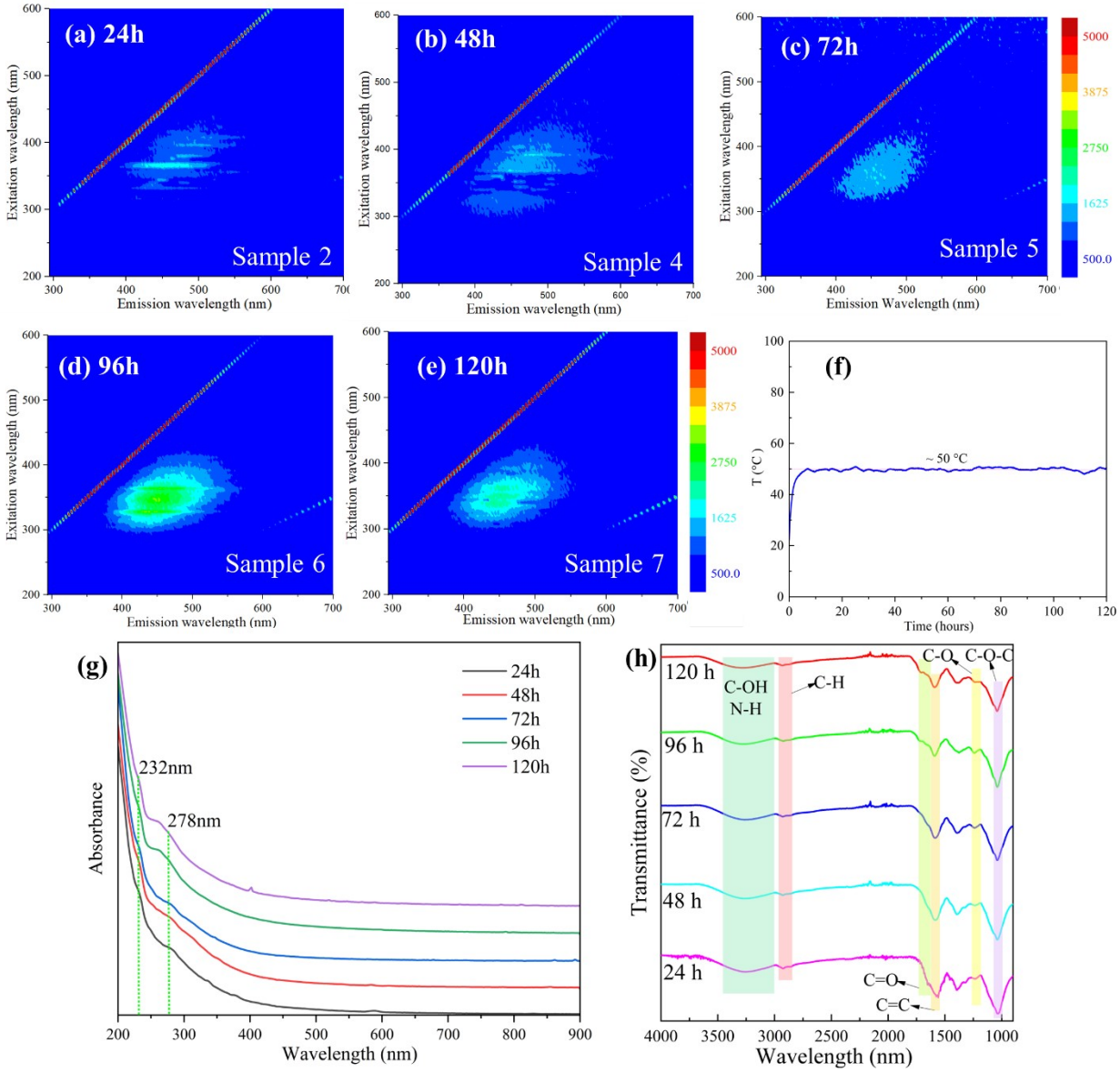

Figure S3. 3D emission-excitation-intensity spectra of CQDs synthesized with the time of (a) 24 h; (b) 48 h; (c) 72 h; (d) 96 h; (e) 120 h; (f) the graph of the temperature within 120 h under the same light intensity (834 mW/cm^2); (g) Comparison of UV-vis absorption spectra of CQDs based on various reaction time; (h) Comparison of ATR-FTIR absorption spectra of CQDs synthesized with different reaction times. (Note: other reaction conditions: 834 mW/cm^2 of light, strong stirring, with an atmosphere environment).

Figure S4. Effect of O_2 flow

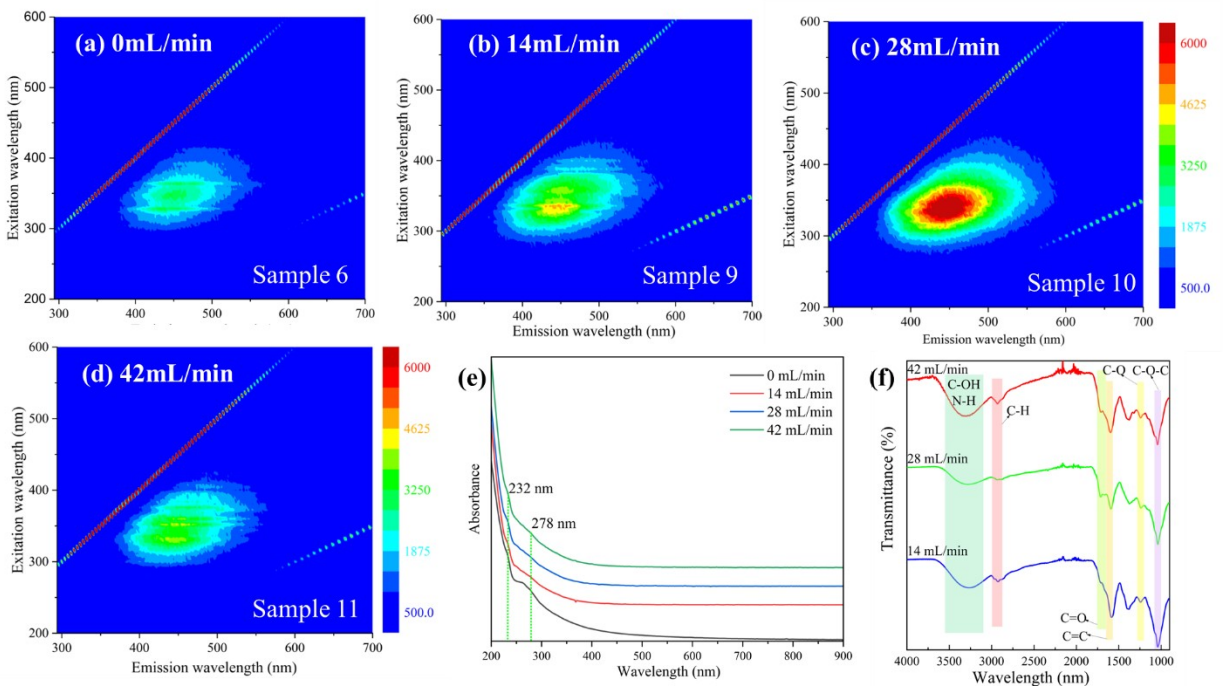

Figure S4. 3D emission-excitation-intensity spectra of CQDs synthesized with the O_2 of (a) 0 mL/min; (b) 14 mL/min; (c) 28 mL/min; (d) 40 mL/min. (Other reaction conditions: 834 mW/cm^2 of light, 96 h of reaction time, strong stirring, with atmosphere environment).

Figure S5. Effect of light wavenumber ranges

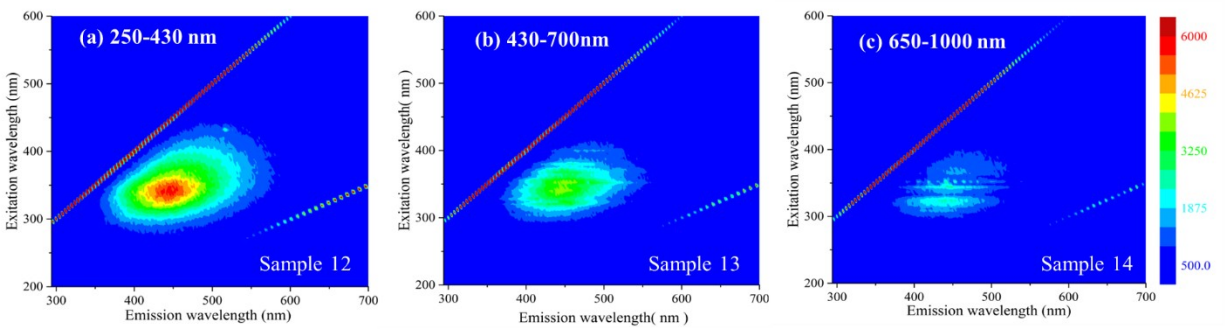

Figure S5 3D emission-excitation-intensity spectra of CQDs synthesized with the different light wavelength ranges of (a) 250-430 nm; (b) 430-700 nm; (c) 650-1000 nm (Other reaction conditions: 96 h of reaction time, 834 mW/cm^2 of light, strong stirring, 27 mL/min of O_2).

Figure S6. Effect of separated components of corn stover

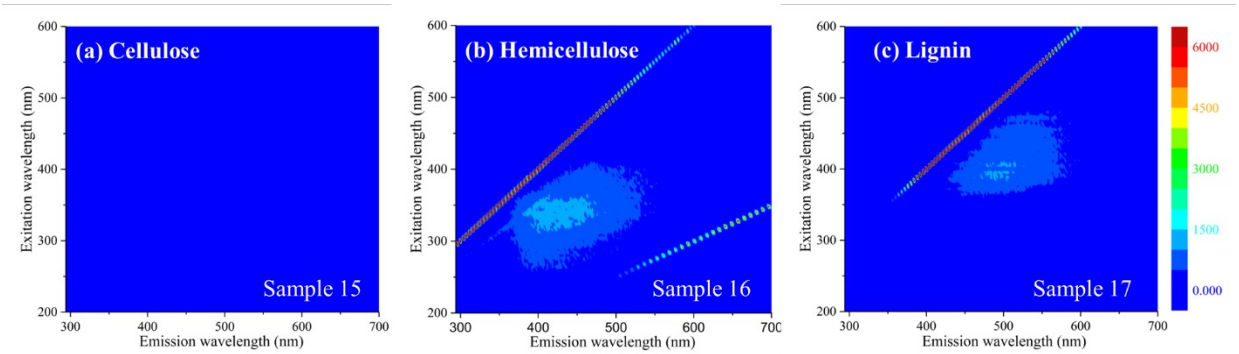

Figure S6 3D emission-excitation-intensity spectra of CQDs synthesized by (a) cellulose, (b) hemicellulose, and (c) lignin with/without light and O_2. (Other reaction conditions: 834 mW/cm^2 of light, 96 h of reaction time, vigorous stirring, 27 mL/min of O_2).

Figure S7. Control experiments

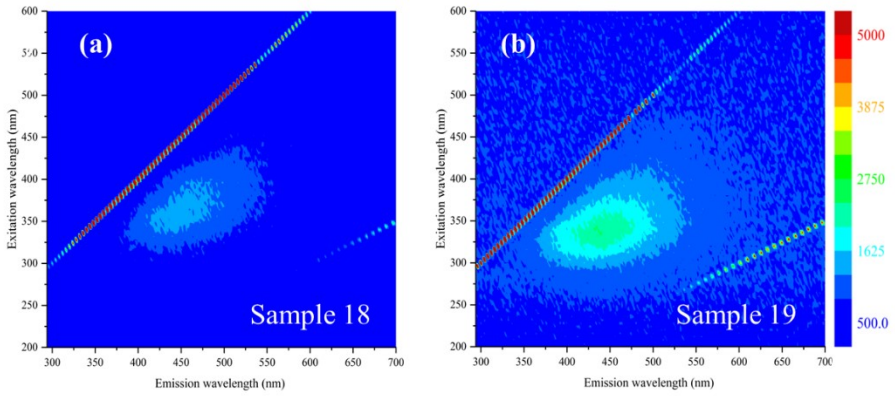

Figure S7 3D-EEM fluorescence spectrum: (a) CQDs prepared with the introduction of O_2 but without light (other reaction conditions: 96 h of time, 28 mL/min of O_2 flow, vigorous stirring); (b) CQDs prepared with simulated solar light and the introduction of N_2 (other reaction conditions: 96 h of time, 28 mL/min of N_2 flow, vigorous stirring).

Figure S8. ESR spectra of H_2O_2 standards and reaction systems under different conditions

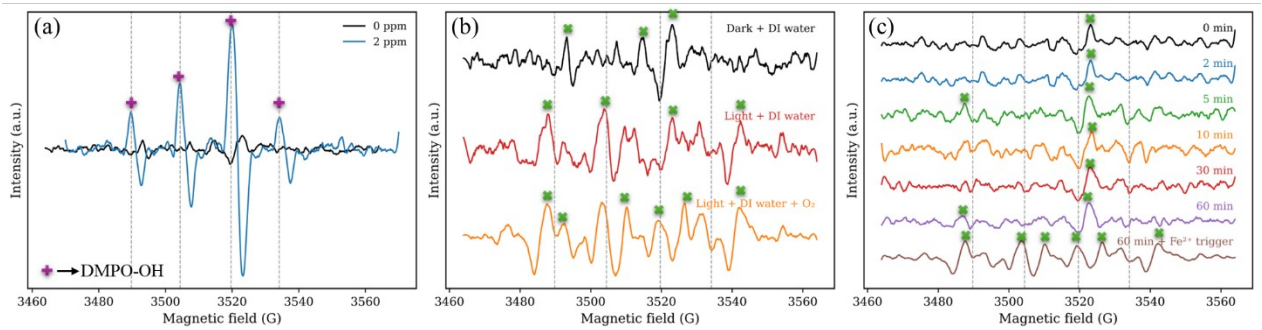

Figure S8. **(a)** ESR spectra of H_2O_2 standards (0 and 2 ppm); **(b)** ESR spectra collected from DI water systems under dark conditions, illumination, and illumination with O_2 flow; **(c)** Time-resolved ESR spectra of filtrates from the corn-stover-containing reaction system under illumination and O_2 flow.

Figure S9. Fluorescent microscopy of CQDs

Fluorescence microscopy was employed to visualize the photoluminescent behavior of the synthesized carbon quantum dots (CQDs) using a ZEISS LSM 700 confocal laser scanning microscope. The results show that the synthesized carbon quantum dots (CQDs) are well-dispersed and exhibit strong photoluminescence under UV light.

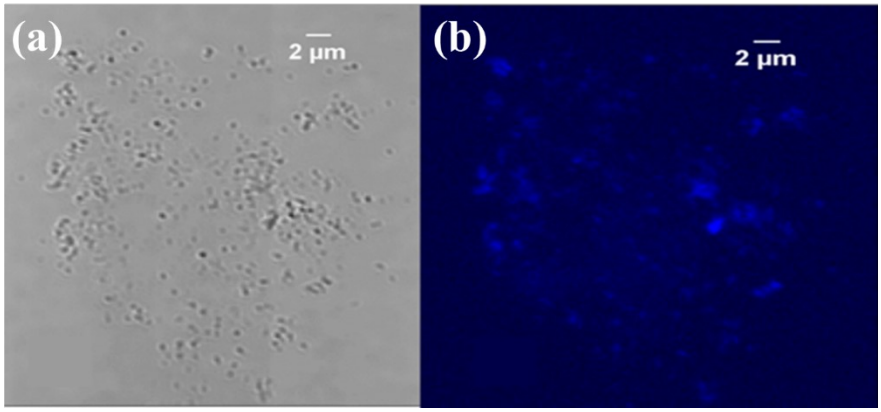

Figure S9. The visible (a) and UV light (b) images of the CQDs by fluorescent microscopy (scale bar: 2 μm)

Figure S10. TGA of corn stover and CQDs

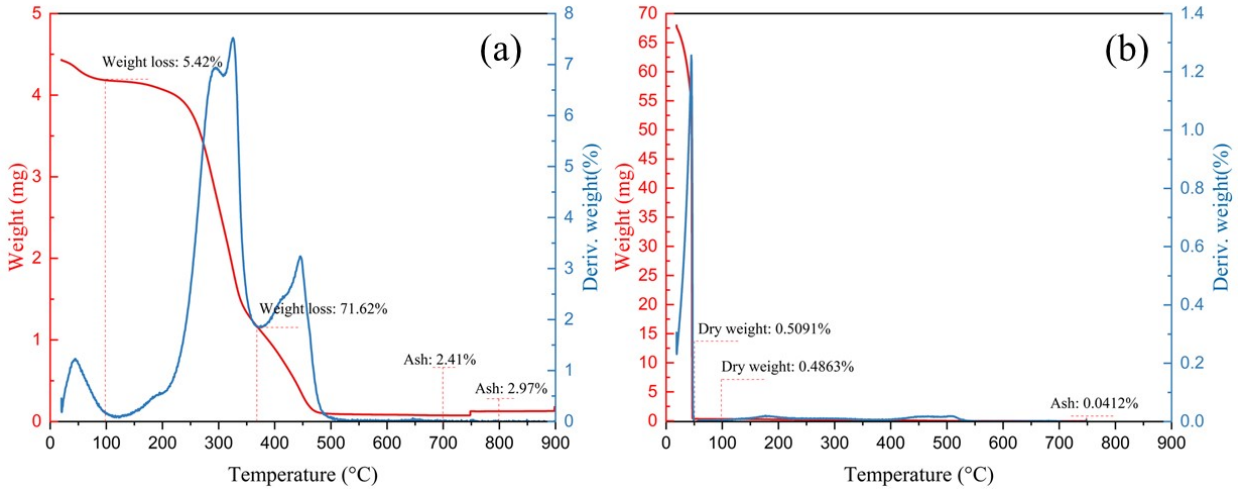

Figure S10. TGA curve of (a) corn stover powder and (b) CQDs (*sample 10*)

Figure S11. LCMS chromatograms of CQDs before and after dialysis

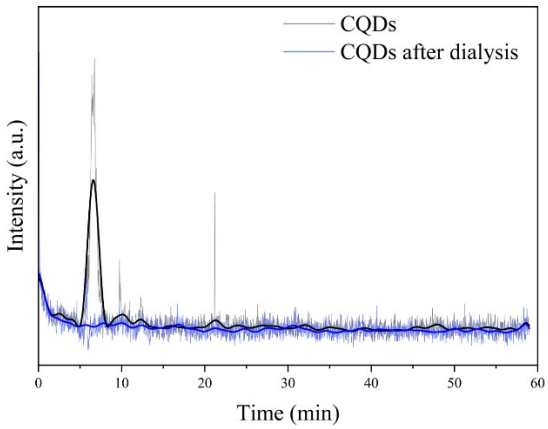

Figure S12. TEM of CQDs after dialysis filtration

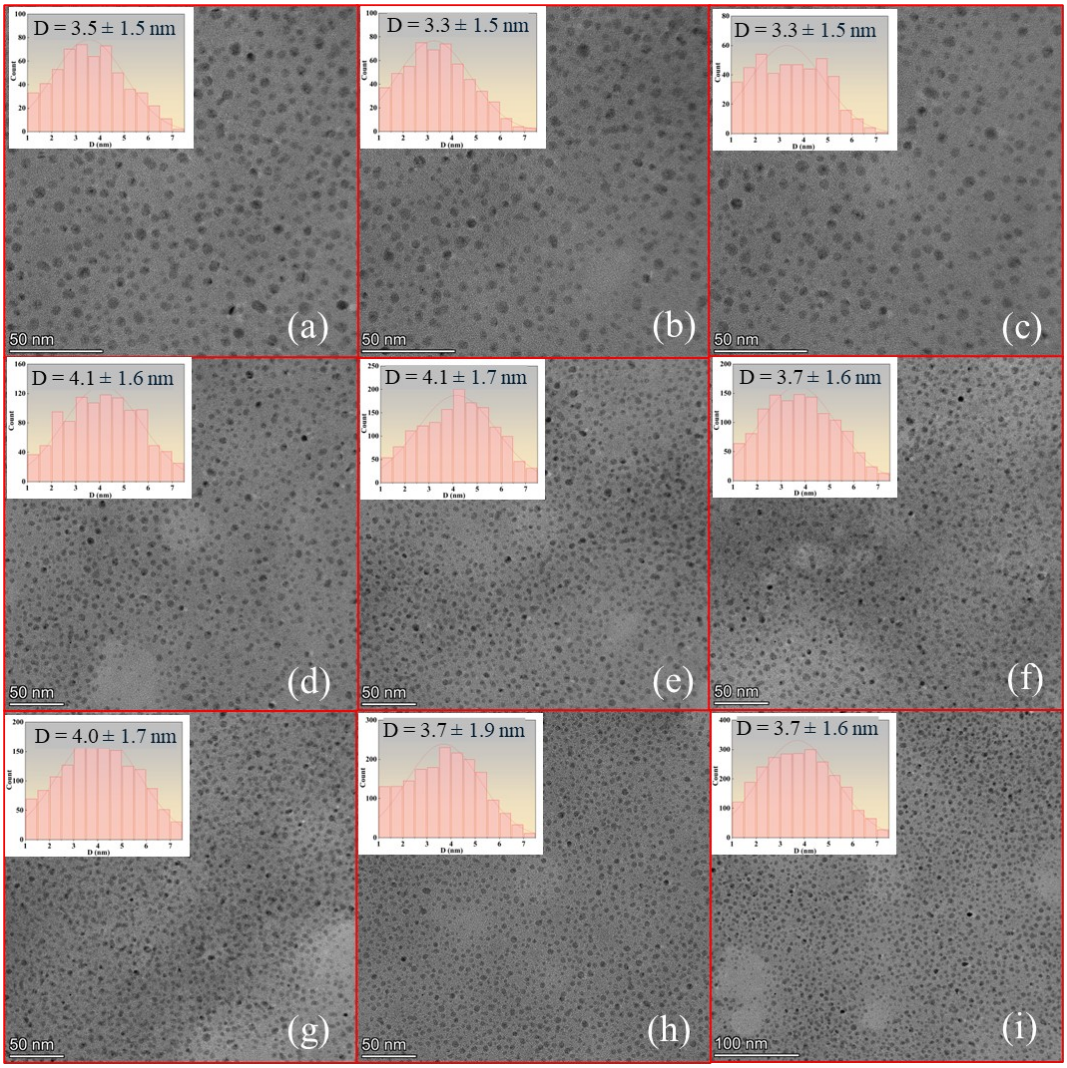

Table S1. Summary of the experimental conditions and the resultant pHs of the corresponding CQDs

Exp.	Carbon resources	Weight (g)	Light intensity (mW cm^{-2})	Reaction time (h)	Atmosphere conditions	Flowrate of O_2 (mL min^{-1})	Wavelength range of light (nm)	pH of aqueous CQDs
Without the introduction of O_2								
Effect of light intensity								
Sample 1	Corn stover	0.5	555	24	WAE	0	>260	6.47
Sample 2	Corn stover	0.5	834	24	WAE	0	>260	6.87
Sample 3	Corn stover	0.5	1050	24	WAE	0	>260	6.36
Effect of reaction time								
Sample 4	Corn stover	0.5	834	48	WAE	0	>260	6.63
Sample 5	Corn stover	0.5	834	72	WAE	0	>260	6.40
Sample 6	Corn stover	0.5	834	96	WAE	0	>260	5.02
Sample 7	Corn stover	0.5	834	120	WAE	0	>260	4.47
Without light (with the temperature of 50℃ by heating and a reaction time of 96h)								
Sample 8	Corn stover	0.5	0 (50℃)	96	WAE	0	/	6.44
With the introduction of O_2								
Effect of O_2 flow rate								
Sample 9	Corn stover	0.5	834 (600W)	96	Rich O_2	14	>260	4.48
Sample 10	Corn stover	0.5	834 (600W)	96	Rich O_2	28	>260	4.09
Sample 11	Corn stover	0.5	834 (600W)	96	Rich O_2	42	>260	3.97
Effect of light wavenumber ranges								
Sample 12	Corn stover	0.5	834 (600W)	96	Rich O_2	28	250-430	5.25
Sample 13	Corn stover	0.5	834 (600W)	96	Rich O_2	28	430-700	6.86
Sample 14	Corn stover	0.5	834 (600W)	96	Rich O_2	28	650-1000	7.05
Effect of separated components of corn stover								
Sample 15	Cellulose	0.5	834 (600W)	96	Rich O_2	28	>260	/
Sample 16	Hemicellulose	0.5	834 (600W)	96	Rich O_2	28	>260	/
Sample 17	Lignin	0.5	834 (600W)	96	Rich O_2	28	>260	/
Control experiments								
Sample 18	Corn stover	0.5	/	96	Rich O_2	28	/	/
Sample 19	Corn stover	0.5	834 (600W)	96	N_2	28	>260	/

WAE: with atmosphere environment.

Table S2. Major elements of corn stover used in this study

No.	Element	(wt%)
1	C	44.62
2	O	46.68
3	H	6.09
4	N	0.75
5	S	1.87

Table S3. Concentrations of various metallic ions in the prepared CQD solutions

Sample	Ag (ppm)	Al (ppm)	Ce (ppm)	Co (ppm)	Cr (ppm)	Cu (ppm)	Fe (ppm)	Mn (ppm)	Mo (ppm)	Ni (ppm)	Pb (ppm)	Ru (ppm)	Ti (ppm)	V (ppm)	W (ppm)
S-6	0.00	0.40	0.00	0.03	0.11	0.32	0.81	0.25	0.02	1.21	0.02	0.22	0.01	0.00	0.01
S-8	0.00	0.16	0.00	0.19	0.03	0.09	0.14	0.11	0.02	0.06	0.02	0.22	0.01	0.01	0.01
S-10	0.00	0.02	0.00	0.01	0.00	0.04	0.28	0.01	0.01	0.05	0.02	0.22	0.01	0.00	0.01

Table S4. Parameters used for quantum yield calculations and the calculated quantum yields of CQDs produced under various conditions

Sample	Integrated emission intensity at 350 nm (I)	Absorbance at 350 nm (A)	Refraction index of solvent (η)	Quantum yield (%)
Qunine sulfate	2596423	0.0525	1.33	54
Sample 6	438828	0.0351	1.33	13.7
Sample 8	352577	0.0428	1.33	9.0
Sample 10-batch 1	613271	0.0333	1.33	20.1
Sample 10-batch 2	460875	0.0241	1.33	20.9
Sample 10-batch 3	540240	0.0305	1.33	19.3
Sample 10 (mean ± SD)	-	-	-	20.1 ± *0.8*

Table S5. Comparison for metallic ions (ICP-MS) and anions (IC) of CQDs after dialysis

Sample	Ag (ppm)	Al (ppm)	Ce (ppm)	Co (ppm)	Cr (ppm)	Cu (ppm)	Fe (ppm)	Mn (ppm)	Mo (ppm)	Ni (ppm)	Pb (ppm)
S-10 after centrifuge and dialysis filtration	0.00	0.04	0.00	0.00	0.01	0.06	0.07	0.02	0.03	0.00	0.00
Sample	Ru (ppm)	Ti (ppm)	V (ppm)	W (ppm)	F^- (ppm)	Cl^- (ppm)	NO_2^- (ppm)	Br^- (ppm)	NO_3^- (ppm)	PO_4^{3-} (ppm)	SO_4^{2-} (ppm)

S-10 after centrifuge and dialysis filtration	0.00	0.00	0.00	0.00	0.00	1.18	0.00	0.00	0.00	0.00	0.53

Table S6. Comparison of raw materials and reaction conditions for producing CQDs with different methods (≥300 °C pyrolysis or two-step treatments or the additions of chemicals), the resultant CQDs sizes, and QY obtained with three different methods [one-point method (OPM), slope method (SM), and absolute method (AM)]

No.	Raw materials	Methods	Solvent	Additives	Reaction conditions	Size (nm)	QY (%)	QY calculation method	Ref.
Part 1									
1	Ziziphus mauritiana seeds	Microwave-assisted pyrolysis	Pure water	NA	750 °C, 12 h +microwave, 20 min	2–4	21.3	NA	10
2	Willow leaves	Pyrolysis	DI water	NA	700 °C, 2 h	1–4	NA	NA	11
3	Fennel seeds	Pyrolysis	DI water	NA	500 °C, 3 h	3.9 ± 0.9	9.5	AM	12
4	Lychee Kernel	Pyrolysis	Water	NA	300 °C, 2 h	1.12	10.6	OPM	13
5	Date palm frond	Carbonization	Water	NA	300 °C, 2 h	3.5	33.7	OPM	14
6	Aloe vera leaf	Carbonization	Distilled water	NA	250 °C, 2 h +ultrasonic, 30 min	1.5–3.7	16.4	OPM	15
7	Hair	Carbonization +hydrothermal	NA	NA	200 °C, 24 h	4.56	10.75	NA	16
8	Mango kernel	Carbonization	NA	NA	300 °C, 0.5 h	6	NA	NA	17
9	Fresh banana peels	Carbonization	NA	NA	microwave, 9 min	NA	22.3%	NA	18
10	Blue algae	Pyrolysis	Water	NA	250 °C, 1 h	1.42	NA	NA	19
Part 2									
8	Rice husk	Pyrolysis	DI water	NaOH	700 °C (2 h) +900 °C (2 h)	3.8	15	OPM	20
9	Mango peels	Carbonization +oxygenolysis	Ultrapure Water	H_2SO_4/ NaOH	300 °C, 2 h	3	8.5 ± 0.2	SM	21
10	Flax straw	Carbonization +hydrothermal	DI water	Ethylenediamine	250°C, 2 h	2.2	20.7	OPM	22
11	Willow catkin	Acid hydrolysis	Ultrapure water	Urea/ H_2SO_4	Burning to ash	7.3	13.3	OPM	23
12	Waste food	Acid hydrolysis	Water	H_2SO_4/HNO_3	Burning to ash	5	28	NA	24
13	Birchwood	Hydrothermal	Water	Methanol/ Pd/C	240 °C, 4 h	5.24	21.7	OPM	25
14	Tobacco leaf	Hydrothermal	Ultrapure water	$C_2H_4(NH_2)_2$	220 °C, 12 h	6.3	13.7	OPM	26
15	Pomelo juice	Hydrothermal	Water	$(NH_4)_2S_2O_8$	200 °C, 12 h	6.7	18.7	OPM	27
16	Coffee grounds	Hydrothermal	Water	$N_2H_4{\cdot}H_2O$	150-200 °C, 6-10 h	1.88	NA	NA	28
17	Rice residue	Hydrothermal	DI water	lysine	200 °C 12 h	2.7	23.48	OPM	29
18	Flour	Hydrothermal	Water	KIO_4/HCl/ HAc/H_2O_2	200 °C, 4 h +120 °C, 8 h	5-8	16.2	AM	30
19	Waste food	Hydrothermal	Ethanol	Oleic acid	200 °C, 1.5 h	4-20	26	OPM	31
20	Lemon peels	Hydrothermal	Water	H_2SO_4	200 °C, 12 h.	1-3	14	OPM	32
21	Tobacco leaves	Hydrothermal	Water	NaOH	200 °C, 3 h	2.14 ± 0.3	27.9	AM	33
22	*Ginkgo biloba L. leaves*	Hydrothermal	DI water	Ethylenediamine	200 °C, ~10 h	2.5-3.5	NA	NA	34
23	Cambuci juice (*Campomanesia phaea*)	Hydrothermal	Distilled water	NH_4OH/NaOH	190 °C, 6 h	3.7	21.3	SM	35
24	Roses	Hydrothermal	Water	Ethylenediamine/ L-cysteine	180 °C, 5 h	4.5 ± 1.5	9.6	NA	36
25	Grass	Hydrothermal	Water	Ethylenediamine	180 °C, 36 h	7–8	7	NA	37

No.	Raw materials	Methods	Solvent	Additives	Reaction conditions	Size (nm)	QY (%)	QY calculation method	Ref.
26	Marigold flower	Hydrothermal	Water	HCl/NaOH	180 °C, 12 h	5.7	NA	NA	[38]
27	Biomass waste	Hydrothermal	Water	Urea/HCl	180 °C, 12 h	6	3.5-14	OPM	[39]
28	Autohydrolyzates (AH) from wheat straw and bamboo	Hydrothermal	Water	Urea	180 °C, 4 h	2-6	13	NA	[40]
29	Pseudo-stem juice of banana plant	Hydrothermal	Water	Ethanol	180°C, 2 h	2-3	48	SM	[41]
30	Laurel leaves	Hydrothermal	Ethanol	HNO_3	180 °C, 5 h	3.8	49.9	OPM	[42]
31	Corncob	Hydrothermal	DI water	Ammonium Water	180 °C, 5 h	NA	NA	NA	[43]
32	Corn straw	Hydrothermal	Water	HNO_3	180 °C, 13 h	~5	4.64	SM	[44]
33	Bael leaves	Hydrothermal	Water	NaOH	170 °C, 5 h	3-8	3	OPM	[45]
34	Pineapple juice	Hydrothermal	Ethanol	CH_2Cl_2	150 °C, 2 h	2–3	42	SM	[46]
35	Saccharum officiarum juice	Hydrothermal	Water	Ethanol	120°C, 3 h	~3	5.67	OPM	[47]
36	*Manilkara zapota fruits*	Hydrothermal	Water	H_3PO_4/H_2SO_4	100 °C, 1 h	1.9 ± 0.3	5.7	OPM	[48]
37	Corn stover	Hydrothermal	DI water	Polytetrafluoroethylene	220 °C, 10 h	2.07	37.4	OPM	[49]
38	Durian seed waste	Hydrothermal	Ultrapure water	Glutamine (Gln)	200 °C, 15 h	2.2	17.24	OPM	[50]
39	Fresh Eucalyptus globulus leaves	Hydrothermal	Distilled water	Citric acid and ethylenediamine	180 °C, 24 h	6.33	60.7	SM	[51]
40	Durian shell	Hydrothermal	DI water	Urea and aluminum nitrate	210 °C, 12 h	10	28.7	OPM	[52]
41	Banana peels	Hydrothermal	DI water and ethanol	NA	200 °C, 24 h	3-6	NA	NA	[53]
42	Waste chicken bones	Hydrothermal	Pure water	NA	180 °C, 4 h	3.2 ± 0.2	NA	NA	[54]
43	Roasted coffee powders	Hydrothermal	DI water	NA	230 °C, 2 h	5-10	NA	NA	[55]
44	Pistachio shell	Hydrothermal	DI water	NA	200 °C, 6 h	NA	9.5	NA	[56]
45	Orange peel	Hydrothermal	Water	Ethylenediamine	180 °C, 3 h	3.5-5.5	35.37	OPM	[57]
46	Corn stover	O_2-rich photo-hydrothermal	DI water	None	Xe lamp (600W), O_2 (28 mL min^{-1}), 96 h	3.1 ± 1.4	20.1 ± 0.8	OPM	This work

Note: NA notes no available; DI water means deionized water.

Table S7. Comparison of raw materials and reaction conditions for producing CQDs via one-step hydrothermal or photothermal treatment with the use of only biomass and H_2O, the resultant CQDs sizes, and quantum yields calculated with the one-point-method (OPM)

No.	Raw materials	Stages of the raw material	Methods	Solvent	Reaction conditions	Size (nm)	Quantum yields (QY, %)	QY calculation method	Ref.
Part 1									
1	Fresh flower of Lantana camara	Fresh	Hydrothermal	Double distilled water	250 °C, 5 h	2.4	29	OPM	[58]

No.	Raw materials	Stages of the raw material	Methods	Solvent	Reaction conditions	Size (nm)	Quantum yields (QY, %)	QY calculation method	Ref.
2	Coriander leaves	Fresh	Hydrothermal	Distilled water	240 °C, 4 h	4.15	6.48	OPM	[59]
3	*Fresh Tamarindus indica leaves*	Fresh	Hydrothermal	Distilled water	210 °C, 5 h	3.4 ± 0.5	46.6	OPM	[60]
4	Fresh Bamboo leaves	Fresh	Hydrothermal	DI water	200 °C, 6 h	2–6	7.1	OPM	[61]
5	Fresh orange peels	Fresh	Hydrothermal	Ultrapure water	200 °C, 4 h	2.34	18.57	OPM	[62]
6	Fresh pomelo peel	Fresh	Hydrothermal	DI water	180 °C, 5 h	5.5	17.3	OPM	[63]
7	Fresh sweet red pepper	Fresh	Hydrothermal	Water	180°C, 5 h	2-7	19.3	OPM	[64]
8	Fresh Cabbage	Fresh	Hydrothermal	Water	140°C, 5 h	2-6	16.5	OPM	[65]
Part 2									
9	Corn stover	Dried	O_2-rich photo-hydrothermal	DI water	Xe lamp (600W), O_2 (28 mL min^{-1}), 96h	3.1 ± 1.4	20.1	OPM	This work
10	Corn stover	Dried	Anoxic Photo-hydrothermal	DI water	Xe lamp (600W), 96h	29.8 ± 13.5	13.7	OPM	This work
11	Corn stover	Dried	Hydrothermal	DI water	50 °C, 96 h	69.4 ± 20.5	10.6	OPM	This work

Table S8. Comparison of raw materials and reaction conditions for producing CQDs via the thermal or photo treatment of externally added H_2O_2 with externally added catalysts; and internally H_2O-generated-H_2O_2 without externally added catalysts.

No.	Raw materials (mg)	Methods	Oxidants	Initial ratio of H_2O_2/C-source-material (mg/mg)	Reaction conditions	Size (nm)	QY(%)	Ref.
1	graphene oxide	Photo-hydrothermal, externally added H_2O_2 photocatalytic oxidation with the use of externally added catalyst)	Fe^{2+}/Fe^{3+} /H_2O_2	136/25	Mercury lamp (365 nm, 1000 W), 15 min	40	NA	[66]
2	graphene oxide	Hydrothermal, externally added H_2O_2 thermal catalytic oxidation with the use of an externally added catalyst	H_2O_2 ($W_{18}O_{49}$ as catalyst)	340/150	200 °C for 72 h	3.4	NA	[67]
3	Corn stover	O_2-rich photo-hydrothermal, internally H_2O-generated H_2O_2 photocatalytic oxidation without the use of externally added catalyst	None	0/500	Xe lamp (600 W), O_2 (28 mL/min), 96 h	3.1 ± 1.4	20.1	This work
4	Corn stover	Anoxic photo-hydrothermal, internally H_2O-generated H_2O_2 photocatalytic oxidation without the use of externally added catalyst	None	0/500	Xe lamp (600W), 96 h	29.8 ± 13.5	13.7	This work
5	Corn stover	Hydrothermal, internally H_2O-generated H_2O_2 thermalcatalytic oxidation without the use of externally added catalyst	None	0/500	50 °C, 96 h	69.4 ± 20.5	9.0	This work

References

1 H. Nie, M. Li, Q. Li, S. Liang, Y. Tan, L. Sheng, W. Shi and S. X. A. Zhang, *Chemistry of Materials*, 2014, 26, 3104–3112.

2 S. Moonrinta, B. Kwon, I. In, S. Kladsomboon, W. Sajomsang and P. Paoprasert, *Opt Mater (Amst)*, 2018, 81, 93–101.

3 B. Al-Hashimi, K. M. Omer and H. S. Rahman, *Arabian Journal of Chemistry*, 2020, 13, 5151–5159.

4 N. B. Mandava, in *Handbook of Natural Pesticides: Methods*, CRC Press, 2019, pp. 219–256.

5 S. Wartewig, *IR and Raman Spectroscopy*, WILEY-VCH, 2003.

6 Y. Shi, X. Liu, M. Wang, J. Huang, X. Jiang, J. Pang, F. Xu and X. Zhang, *Int J Biol Macromol*, 2019, 128, 537–545.

7 Y. Liu and J. Wang, *Chemical Engineering Journal*, 2023, 466, 143147.

8 S. Hussain, E. Aneggi and D. Goi, *Environ Chem Lett*, 2021, 19, 2045–2424.

9 D. Xu, Y. Li, N. Li, F. Lei, J. Liu, Y. Shi, L. Yin and L. Zhang, *Nano Express*, 2020, 1, 020001.

10 S. Ganesan, R. Kalimuthu, T. Kanagaraj, R. Kulandaivelu, R. Nagappan, L. A. Pragasan and V. K. Ponnusamy, *Environ Res*, 2022, 206, 112589.

11 S. Gao, Y. Chen, H. Fan, X. Wei, C. Hu, L. Wang and L. Qu, *J Mater Chem A Mater*, 2014, 2, 6320–6325.

12 A. Dager, T. Uchida, T. Maekawa and M. Tachibana, *Sci Rep*, 2019, 9, 14004.

13 M. Xue, M. Zou, J. Zhao, Z. Zhan and S. Zhao, *J Mater Chem B*, 2015, 3, 6783–6789.

14 T. Kavitha and S. Kumar, *Sci Rep*, 2018, 8, 16269.

15 N. Sarkar, G. Sahoo, R. Das, G. Prusty and S. K. Swain, *European Journal of Pharmaceutical Sciences*, 2017, 109, 359–371.

16 Y. Guo, L. Zhang, F. Cao and Y. Leng, *Sci Rep*, 2016, 6, 35795.

17 S. Saini, K. Kumar, P. Saini, D. K. Mahawar, K. S. Rathore, S. Kumar, A. Dandia and V. Parewa, *RSC Adv*, 2022, 12, 32619–32629.

18 H. K. Thabet, A. M. Ashmawy, A. I. Hosameldin and A. M. Abdel-Raoof, *Microchemical Journal*, 2025, 216, 114700.

19 S. Chen, S. Z. Zhang and H. Jiang, *ACS ES and T Water*, 2024, 4, 531–542.

20 Z. Wang, J. Yu, X. Zhang, N. Li, B. Liu, Y. Li, Y. Wang, W. Wang, Y. Li, L. Zhang, S. Dissanayake, S. L. Suib and L. Sun, *ACS Appl Mater Interfaces*, 2016, 8, 1434–1439.

21 X. Y. Jiao, L. shuang Li, S. Qin, Y. Zhang, K. Huang and L. Xu, *Colloids Surf A Physicochem Eng Asp*, 2019, 577, 306–314.

22 G. Hu, L. Ge, Y. Li, M. Mukhtar, B. Shen, D. Yang and J. Li, *J Colloid Interface Sci*, 2020, 579, 96–108.

23 C. Cheng, M. Xing and Q. Wu, *Materials Science and Engineering C*, 2019, 99, 611–619.

24 Y. Zhou, Y. Liu, Y. Li, Z. He, Q. Xu, Y. Chen, J. Street, H. Guo and M. Nelles, *RSC Adv*, 2018, 8, 23657–23662.

25 X. Chen, J. Zhu, W. Song and L. P. Xiao, *Front Bioeng Biotechnol*, 2021, 9, 803138.

26 Y. M. Liang, H. Yang, B. Zhou, Y. Chen, M. Yang, K. S. Wei, X. F. Yan and C. Kang, *Anal Chim Acta*, 2022, 1191, 339269.

27 J. Shen, S. Shang, X. Chen, D. Wang and Y. Cai, *Sens Actuators B Chem*, 2017, 248, 92–100.

28 L. Wang, W. Li, B. Wu, Z. Li, S. Wang, Y. Liu, D. Pan and M. Wu, *Chemical Engineering Journal*, 2016, 300, 75–82.

29 H. Qi, M. Teng, M. Liu, S. Liu, J. Li, H. Yu, C. Teng, Z. Huang, H. Liu, Q. Shao, A. Umar, T. Ding, Q. Gao and Z. Guo, *J Colloid Interface Sci*, 2019, 539, 332–341.

30 Z. Zhang, Y. Duan, Y. Yu, Z. Yan and J. Chen, *J Mater Sci Mater Med*, 2015, 26, 1–7.

31 P. K. Sarswat and M. L. Free, *Physical Chemistry Chemical Physics*, 2015, 17, 27642–27652.

32 A. Tyagi, K. M. Tripathi, N. Singh, S. Choudhary and R. K. Gupta, *RSC Adv*, 2016, 6, 72423–72432.

33 H. Miao, Y. Wang and X. Yang, *Nanoscale*, 2018, 10, 8139–8145.

34 J. C. Fei and S. W. Sun, *Biomass Convers Biorefin*, 2024, 14, 21695–21703.

35 A. H. da Silva Júnior, D. Lusitâneo Pier Macuvele, H. Gracher Riella, C. Soares and N. Padoin, *Mater Lett*, 2021, 283, 128813.

36 V. Sharma, S. K. Singh and S. M. Mobin, *Nanoscale Adv*, 2019, 1, 1290–1296.

37 P. Krishnaiah, R. Atchudan, S. Perumal, E. S. Salama, Y. R. Lee and B. H. Jeon, *Chemosphere*, 2022, 286, 131764.

38 G. K. Gupta, P. Sagar, M. Srivastava, A. K. Singh, J. Singh, S. K. Srivastava and A. Srivastava, *Int J Hydrogen Energy*, 2021, 46, 38416–38424.

39 Ł. Janus, J. Radwan-Pragłowska, M. Piatkowski and D. Bogdał, *Materials*, 2020, 13, 3313.

40 C. Huang, H. Dong, Y. Su, Y. Wu, R. Narron and Q. Yong, *Nanomaterials*, 2019, 9, 387.

41 S. A. A. Vandarkuzhali, V. Jeyalakshmi, G. Sivaraman, S. Singaravadivel, K. R. Krishnamurthy and B. Viswanathan, *Sens Actuators B Chem*, 2017, 252, 894–900.

42 X. Long, J. Wang, Y. Ma and S. Wu, *Colloids Surf A Physicochem Eng Asp*, 2023, 676, 132136.

43 L. Zhang, Y. Wang, W. Liu, Y. Ni and Q. Hou, *Ind Crops Prod*, 2019, 133, 18–25.

44 J. Yang, Z. Guo and X. Yue, *Bioresources*, 2022, 17, 604–615.

45 A. Pramanik, S. Biswas and P. Kumbhakar, *Spectrochim Acta A Mol Biomol Spectrosc*, 2018, 191, 498–512.

46 S. A. A. Vandarkuzhali, S. Natarajan, S. Jeyabalan, G. Sivaraman, S. Singaravadivel, S. Muthusubramanian and B. Viswanathan, *ACS Omega*, 2018, 3, 12584–12592.

47 V. N. Mehta, S. Jha and S. K. Kailasa, *Materials Science and Engineering C*, 2014, 38, 20–27.

48 J. R. Bhamore, S. Jha, T. J. Park and S. K. Kailasa, *J Photochem Photobiol B*, 2019, 191, 150–155.

49 J. Wang, D. Han and Z. Yan, *Spectroscopy Letters*, 2024, 57, 428–441.

50 M. Zulfajri, S. Sudewi, A. Rasool, S. C. N. Hsu and G. G. Huang, *Waste Biomass Valorization*, 2023, 14, 3971–3986.

51 A. Johny, L. Pinto da Silva, C. M. Pereira and J. C. G. Esteves da Silva, *Environments*, 2024, 11, 6.

52 S. Jayaweera, K. Yin, X. Hu and W. J. Ng, *J Fluoresc*, 2019, 29, 1291–1300.

53 T. N. Nguyen, P. A. Le and V. B. T. Phung, *Biomass Convers Biorefin*, 2022, 12, 2407–2416.

54 H. Ye, B. Liu, J. Wang, C. Zhou, Z. Xiong and L. Zhao, *Molecules*, DOI:10.3390/molecules27196479.

55 L. Yao, M. M. Zhao, Q. W. Luo, Y. C. Zhang, T. T. Liu, Z. Yang, M. Liao, P. Tu and K. W. Zeng, *ACS Nano*, 2022, 16, 9228–9239.

56 N. Manjubaashini, P. Bargavi and S. Balakumar, *J Photochem Photobiol A Chem*, 2024, 454, 115702.

57 L. Han, Y. Guo, H. Zhang, Z. Wang, F. Zhang, Y. Wang, X. Li, Y. Wang and J. Ye, *RSC Adv*, 2024, 14, 1813–1821.

58 V. K. Mahto, V. K. Singh, V. K. Singh, A. Singh, S. Singh, A. K. Mehara, N. Rajak, A. Mishra, N. Garg, A. Upadhyay, A. Rai and A. K. Singh, *Biomass Convers Biorefin*, 2024, 15, 16857–16870.

59 A. Sachdev and P. Gopinath, *Analyst*, 2015, 140, 4260–4269.

60 D. Bano, V. Kumar, V. K. Singh and S. H. Hasan, *New Journal of Chemistry*, 2018, 42, 5814–5821.

61 Y. Liu, Y. Zhao and Y. Zhang, *Sens Actuators B Chem*, 2014, 196, 647–652.

62 M. Wang, R. Shi, M. Gao, K. Zhang, L. Deng, Q. Fu, L. Wang and D. Gao, *Food Chem*, 2020, 318, 126506.

63 D. Zhang, F. Zhang, Y. Liao, F. Wang and H. Liu, *Molecules*, 2022, 27, 4099.

64 B. Yin, J. Deng, X. Peng, Q. Long, J. Zhao, Q. Lu, Q. Chen, H. Li, H. Tang, Y. Zhang and S. Yao, *Analyst*, 2013, 138, 6551–6557.

65 A. M. Alam, B. Y. Park, Z. K. Ghouri, M. Park and H. Y. Kim, *Green Chemistry*, 2015, 17, 3791–3797.

66 X. Zhou, Y. Zhang, C. Wang, X. Wu, Y. Yang, B. Zheng, H. Wu, S. Guo and J. Zhang, *ACS Nano*, 2012, 6, 6592–6599.

67 C. Zhu, S. Yang, G. Wang, R. Mo, P. He, J. Sun, Z. Di, Z. Kang, N. Yuan, J. Ding, G. Ding and X. Xie, *J Mater Chem B*, 2015, 3, 6871–6876.